02 Apr 2007

# Computational Study of Laminar Separation Bubble Development over Supersonic Airfoils at Subsonic Speeds

Josiah D. Elliott

**Josiah D. Elliott**

# Computational Study of Laminar Separation Bubble Development over Supersonic Airfoils at Subsonic Speeds

Advisor: Dr. Fathi Finaish
Department of Aerospace Engineering
April 2, 2007

**[Abstract] Laminar Separation Bubbles (LSBs) are regions of separated flow that start near the leading edge of an airfoil and reattach further down the airfoil surface. These regions of separation can appear at low angles of attack and can grow significantly as the angle of attack is increased heavily influencing the flow characteristics over the airfoil. Research on this topic is driven by the supersonic business jet industry which has a particular interest in this type of research due to performance requirements in both the subsonic and supersonic flight regimes. This manuscript is focused on the flow developments near the sharp leading edge of supersonic airfoils and their influence on aerodynamic performance at low subsonic speeds. Computational Fluid Dynamics was utilized to show how LSB formation, size, and shape are dependent on the turbulence model chosen and the level of free-stream turbulence present in the flow. Two turbulence models were investigated, the Spalart-Allmaras and the Menter's SST. The LSB modeled by the Spalart-Allmaras turbulence model was consistently longer than the LSB modeled by the Menter's SST turbulence model. Both models verified the LSB dependence on the Reynolds and Mach number of the flow.**

## I. Introduction

THIS manuscript details research performed to investigate the dependence of modeling Laminar Separation Bubbles (LSBs) on the choice of turbulence model and the level of free-stream turbulence present in a flow. A description of LSBs is presented in the next section. The paper is focused on the flow developments near the sharp leading edge of supersonic airfoils and their influence on aerodynamic performance at subsonic speeds. The motivation for this research comes from the supersonic business jet industry which has a particular interest in this type of research due to performance requirements in both the subsonic and supersonic flight regimes. The goal of the project was to use Computational Fluid Dynamics (CFD) to show how the LSB formation, size, and shape are affected by the turbulence model chosen and the level of free-stream turbulence present in the flow. From this goal a better understanding of the behavior and CFD analysis of LSBs is expected. This project investigated two prominent turbulence models, the Spalart-Allmaras and the Menter's SST. Two primary parameters were varied in this analysis, the turbulence intensity and the Mach number in the free-stream flow. For each Mach number analyzed a new Reynolds number was calculated based on the corresponding velocity, and the trends of the LSB dimensions with respect to Reynolds and Mach number were verified. A comparison between the two turbulence models (with no free-stream turbulence present) and their ability to predict the development of an LSB and the dimensional change associated with a change in Reynolds and Mach number was made. It was shown that significant dependence exists on the turbulence model chosen. As it will be made clear in subsequent sections of this manuscript, the effect of free-stream turbulence on LSB development was not gleaned in this research. Several issues associated with modeling free-stream turbulence have been identified and significant research into these issues has been performed to allow further investigation. This information is presented in the Results section of this manuscript.

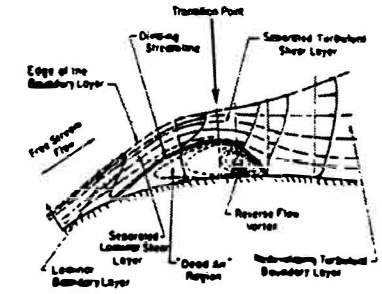

a)

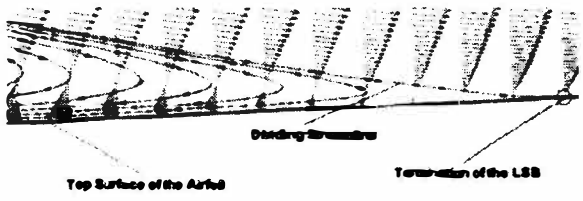

b)

**Figure 1. Laminar Separation Bubbles.**
*a) Generic LSB Illustration (from Ref. 2)*
*b) CFD Generated LSB (velocity profiles and streamlines)*

## II. Overview of Laminar Separation Bubbles

Laminar Separation Bubbles are regions of separated flow that start near the leading edge of an airfoil and reattach further downstream on the airfoil surface. There are two primary ways in which LSBs can form. The first method is adverse pressure gradient (APG) induced separation. In this method a LSB forms in the boundary layer when the oncoming flow encounters an APG. A separated laminar shear layer is then formed producing the LSB. Near the maximum thickness location of the LSB the flow transitions from laminar to turbulent converting the separated laminar shear layer to a separated turbulent shear layer. The flow becomes energized in this region, and it reattaches to the airfoil surface. Downstream from the reattachment point the flow remains turbulent.[1] The second method by which LSBs can form is from geometry induced separation. In this method the separation is caused by sharp gradients in the geometry rather than an APG. The LSBs studied in this research will be characterized by this type of

separation due to the sharp leading edges of the supersonic airfoil studied. An example of a LSB is shown in Fig. 1a[2],b. Figure 1b was generated from the CFD analysis performed in this project. The blue vectors represent the velocity profiles along the airfoil, and several streamlines have been plotted as well. The recirculation inside the bubble can be seen by examination of both the velocity profiles and streamlines. The dividing streamline and the termination point of the LSB are also clearly shown. Regardless of the method that forms them, these regions of separation can appear at low angles of attack and can grow significantly as the angle of attack is increased, heavily influencing the flow characteristics over the airfoil. The size and shape of the bubble can have adverse effects on the performance characteristics of an airfoil. Several factors, such as Mach and Reynolds number and free-stream turbulence[2], can affect the size and shape of an LSB. The level of dependence on free-stream turbulence was one of the desired outcomes for this project.

## III. Turbulence Modeling Methods Employed in This Study

Several turbulence modeling options are available in OVERFLOW, the CFD flow solver utilized in this study. These options include both one and two equation models. The turbulence models selected for this study were the Spalart-Allmaras (SA) and the Menter's SST (Shear Stress Transport) turbulence models. Turbulence models in CFD are applied in two main ways. The first is to model turbulence that would arise naturally around certain flow and geometric features present in the flow. This function of the turbulence model is always active, and remains unchanged by the user in this study. The second way that the turbulence model is utilized is to change the free-stream turbulence present in the flow before any interactions with the airfoil are present.

### A. Spalart-Allmaras[3]

The SA turbulence model is a prominent one equation turbulence modeling option incorporated into OVERFLOW. There are two primary ways to use the SA turbulence model in OVERFLOW, fully turbulent or trip line specification. The fully turbulent option was used in this project which does not imply that the flow is actually turbulent everywhere, but that the turbulence model is active at all points in the flow (i.e. no regions are forced to be laminar). Whether the flow is turbulent or not at a given location is dependent on several factors and can be controlled in part by inputs such as the free-stream turbulence or other internally calculated parameters.

Free-stream turbulence levels are set in the SA model by modifying the turbulent viscosity ratio defined by $(\mu_t/\mu)$. This parameter is the ratio between turbulent eddy viscosity $(\mu_t)$ and the molecular dynamic viscosity $(\mu)$. As this ratio is increased, the turbulent viscosity begins to overcome the molecular viscosity and the flow becomes more turbulent. A reasonable range of values for the turbulent viscosity ratio when applied to free-stream turbulence levels is on the order of $1 < (\mu_t/\mu) < 10$. This range is good for most wind tunnel applications, and lower values of the turbulent viscosity ratio on the order of 0.1 or 0.2 are reasonable for most low speed, external free-stream flows.[8,9] The majority of the cases run in this project fell in the range of $0.1 < (\mu_t/\mu) < 10$. Turbulent viscosity ratios can exist that are much larger, on the order of 100 or greater in regions of high turbulence, and several cases were run with values on this order of magnitude to access the impact this kind of turbulence level has on the LSB.

### B. Menter's SST[4]

The Menter's SST turbulence model is a well known two equation turbulence model. Two equation turbulence models contain two transport equations to represent the turbulent properties of the flow. The two transported variables in this model are k, the kinetic turbulent energy, and $\omega$, the specific dissipation. The SST model is an improvement over the baseline model (BSL) which uses the original Wilcox k-$\omega$ model in the inner region of the boundary layer and switches to the standard k-$\varepsilon$ model in the outer region and in the free shear flow region. The SST model accounts for the effect of the transport of the principle turbulent shear stress.

Free-stream turbulence levels in the SST model can be adjusted by adjusting the level of turbulent kinetic energy (k) present in the flow. A common method of stating the level of turbulence present in a flow is by turbulence intensity (I) reported as a percentage. These two parameters, k and I, can be related by the following sequence of equations. The prime (') in these equations denotes the variation in the velocity above and below the average velocity as is illustrated by the following: $u = u' + u_{avg}, v = v' + v_{avg}$, *and* $w = w' + w_{avg}$

$$I = \frac{U'}{U_{avg}} \tag{1}$$

$$U' = \sqrt{\frac{1}{3}\left(u'^2 + v'^2 + w'^2\right)} \tag{2}$$

$$U_{avg} = \sqrt{u_{avg}{}^2 + v_{avg}{}^2 + w_{avg}{}^2} \tag{3}$$

$$k = \frac{1}{2}\left(\overline{u'^2} + \overline{v'^2} + \overline{w'^2}\right) \tag{4}$$

$$U' = \sqrt{\frac{2}{3}k} \tag{5}$$

$$k = \frac{3}{2}\left(I \cdot U_{avg}\right)^2 \tag{6}$$

Equation (6) was used to calculate turbulent kinetic energy values for turbulence intensities corresponding to 0.8%, 2%, and 10%. Modern wind tunnels can produce levels of turbulence less than 1%, and turbulence intensities higher than 10% are typically considered high.[8,9] The values of turbulent kinetic energy were divided by the square of the free-stream velocity to non-dimensionalize the parameter, a requirement of the turbulence model in OVERFLOW, producing inputs of 0.0001, 0.0005, and 0.015 respectively for the non-dimensional turbulent kinetic energy.

**Figure 2. 4.23% Thick Double Wedge Airfoil**

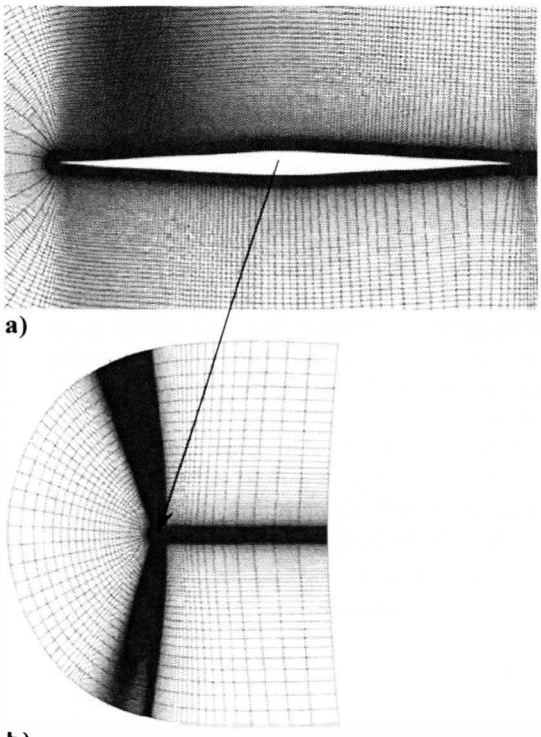

a)

b)

**Figure 3. Volume Grid.** *a) Zoomed in view of the volume grid point distribution b)C grid*

## IV. Grid Generation and Computational Procedure

The following section outlines the procedure used for the CFD analysis in this project. A description of the various software packages utilized is also included. This research was performed on a sharp leading edge, 4.23% thick double wedge airfoil. Note: The following sections refer to surface and volume grid generation. The same naming convention for grids is upheld for either 2D or 3D analysis. This analysis was performed as a 2D analysis, and as such, the surface grid refers to the grid points discretized around the boundary of the airfoil. The volume grid refers to the grid grown outward (normal to the airfoil boundary) in the same plane as the airfoil. Further clarification is made in the following sections, and images of the airfoil and grid are provided.

### A. Geometry and Surface Grid Generation

The first step in the analysis was to generate the airfoil geometry and surface grid. Boeing's Aero Grid and Paneling System[5] (AGPS) provided the tools necessary for this portion of the analysis. The geometry of the airfoil can be seen in Fig. 2. Four Hundred points were extracted around edge of the airfoil using separate spacing rules on the top and bottom curves. This variation in the spacing rule produced more grid resolution near the leading, top edge of the airfoil. To attain this type of grid distribution using AGPS a hyperbolic tangent spacing function with end spacing parameters of 0.02 (top) and 0.01 (bottom) was utilized. Top front clustering has been shown to produce the best results when compared to experimental data versus a symmetric (top and bottom) front clustering and a uniform clustering over

the entire boundary of the airfoil.[1] The increased grid resolution near the area of interest, the LSB, allows for more accurate resolution of this flow feature without producing excessive grid resolution in less critical areas of the flow. The distribution of grid points along the boundary of the airfoil can be seen in Fig. 3a by observing the spacing between the lines normal to the airfoil surface in the volume grid. Once the surface grid was generated, the airfoil section and corresponding grid points were copied and translated one chord length on either side of the original airfoil. This created three parallel planes (2 symmetric planes to the original) from which the volume grid will be grown. This is the standard procedure for running 2D cases in OVERFLOW, the flow solver used for this analysis which is discussed in section C.

### B. Volume Grid Generation

Once the surface grids were generated, Hypgen,[6] a component of the NASA's Chimera Grid Tools software package, was used to create the structured volume grid. Hypgen uses hyperbolic stepping functions to calculate the grid spacing and generate the various volume grid levels. A C grid was generated for this analysis extending to 20 chord lengths in all directions. A wake of 20 chord lengths containing forty points was created behind the airfoil symmetry planes to provide the spacing for the grid behind the airfoil. Fig. 3a provides a zoomed in view of the volume grid showing the distribution of the grid points around the airfoil. Fig. 3b is the entire volume grid (C grid) with the airfoil located at the center of the dense regions as indicated by the arrow.

### C. Flow Solver and Parameter Range Considered

The flow solver used in this research is NASA's OVERFLOW.[7] The code (compiled for serial processing) was run on a single processor PC with 8 megabytes of RAM running Enterprise Linux. OVERFLOW is a Reynolds-Averaged Navier-Stokes (RANS) flow solver. It can solve time accurate RANS equations using several numerical schemes. With the low Mach numbers used in this study, OVERFLOW's low mach preconditioning setting had to be utilized to achieve good results. Three Mach numbers were examined (0.17, 0.3, and 0.5) and the three corresponding Reynolds numbers were calculated ($1.21 \times 10^6$, $2.13 \times 10^6$, and $3.55 \times 10^6$). For each Mach number a range of turbulence parameters were run. The actual parameters and their values are discussed further in the Results section of this manuscript. The Reynolds numbers calculated for the various cases were calculated using Eq. (7).

$$R_e = \frac{\rho c U_\infty}{\mu} \tag{7}$$

The chord length (c) used in the calculation was equal to one and the values for density and molecular dynamic viscosity were the standard sea level values as defined in the Nomenclature section. The free-stream velocity, $U_\infty$, was calculated with Eq. (8).

$$U_\infty = M_\infty \cdot \sqrt{\gamma \cdot R \cdot T_\infty} \tag{8}$$

The proper execution of OVERFLOW requires many inputs that have not been specified or detailed in this manuscript. For a complete list of input parameters see Ref. 7.

## V. Results and Discussion

This portion of the manuscript presents the results obtained from the analysis described in the above sections. The first section compares the results from the two turbulence models, and their level of agreement with respect to the dimensions of the LSB modeled by each. This section also confirms the dependence of a LSB on the Reynolds and Mach number of a flow. The second section discusses the results obtained from analyzing the effect that free-stream turbulence has on a LSB.

### A. Turbulence Model Comparison and Reynolds Number Dependence

Important trends were observed regarding the turbulence models utilized in this study and how they model LSBs. The dependence of the separation bubble on the Reynolds and Mach number was also verified. The following equations were used to calculate the parameters utilized this portion of the analysis.

$$D = \sqrt{(x_2 - x_1)^2 + (y_2 - y_1)^2 + (z_2 - z_1)^2}$$

where 1 → separation point

2 → re-attachment point (9)

$$L = \frac{D}{Chord} \tag{10}$$

$$\%Change = \frac{L_{new} - L_{old}}{L_{new}} \cdot 100 \tag{11}$$

The linear distance from the separation point of the bubble to the reattachment point is represented by D. The coordinates used in Eq. (9) were obtained by plotting streamlines in Tecplot, zooming in extremely close the separation and reattachment points, and using the probe tool to obtain the coordinate data. This method produced good results when the zoom factor was set such that the variation in the choice of separating streamlines was < 0.001 of the normalized chord (x/c) where x is a position along the chord and c is the chord length. Once the distance between the separation and reattachment points was known, Eq. (10) was used to calculate the new normalized length of the bubble represented by L. The final parameter used in this portion of the analysis was the % change in the length of the bubble as the flow's Reynolds and Mach number were increased. This parameter was calculated in Eq. (11).

The non-dimensional length (L) and % change of L as the Mach and Reynolds number are increased for each turbulence model are shown in Table 1 below. These values are without any free-stream turbulence present in the flow.

**Table 1. Comparison Between SA and Menter's SST Turbulence Models; LSB Size Dependence on Free-stream Mach and Reynolds Number.**

| | M = 0.17 $R_e$ = 1,207,455 | | M= 0.3 $R_e$ = 2,130,803 | | M = 0.5 $R_e$ = 3,551,338 | |
|---|---|---|---|---|---|---|
| Model | L | - | L | % Change | L | % Change |
| SA | 0.2182 | - | 0.2279 | 4.4409 | 0.2557 | 12.2031 |
| Menter's SST | 0.1670 | - | 0.1713 | 2.5576 | 0.1875 | 9.4643 |

It can be observed from Table 1 that there is a significant difference in the way LSBs are modeled between the two turbulence models. The length (L) of the LSB is modeled significantly larger with the SA turbulence model than with the Menter's SST. The % change in the LSB's length is also much larger with the SA turbulence model as the Mach and Reynolds number is increased. These trends show that the choice of turbulence model can have a significant impact on the way an LSB is modeled in CFD.

The pressure plots contained in Fig. 4a-f and 5a-c plot the coefficient of pressure ($C_P$). The plots visually illustrate the trends shown above in Table 1. Special attention should be given to the scale of the vertical axis in plots in Fig. 5a-c before making comparisons between plots. The top portion of each curve represents the suction (negative $C_P$ values) or top side of the airfoil and the bottom portion of the airfoil is represented by the bottom curve. The $C_P$ plots in Fig. 5a-c are all versus the normalized chord (x/c) length where zero corresponds to the leading edge, and one corresponds to the trailing edge of the airfoil. These plots were generated without the free-stream turbulence parameters engaged. They are labeled with the appropriate turbulence model, Mach, and Reynolds number. All plots were created using the same zoom and view extents. Accordingly, visual comparison can be made to evaluate the dimensions of the bubble qualitatively.

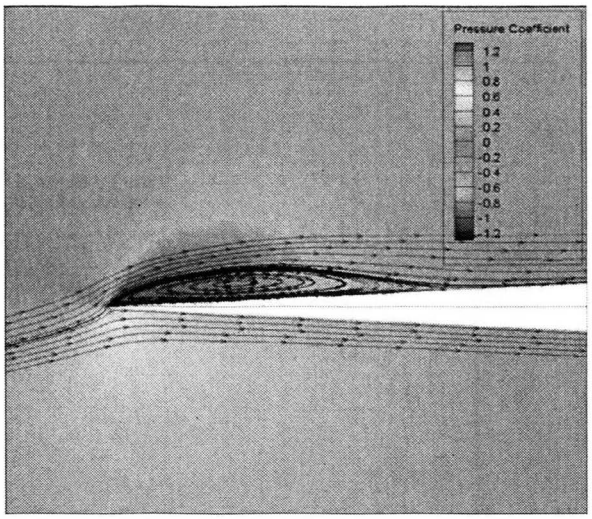


a) M=0.17, Re=1,207,455 SA Turb. Model

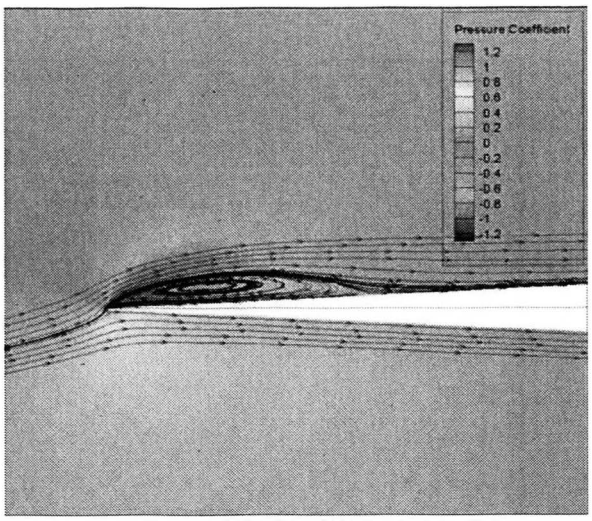


b) M=0.17, Re=1,207,455 SST Turb. Model

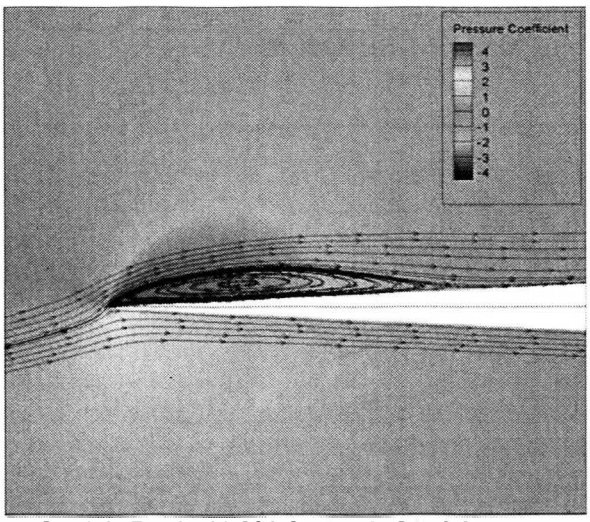


c) M=0.3, Re=2,130,803 SA Turb. Model

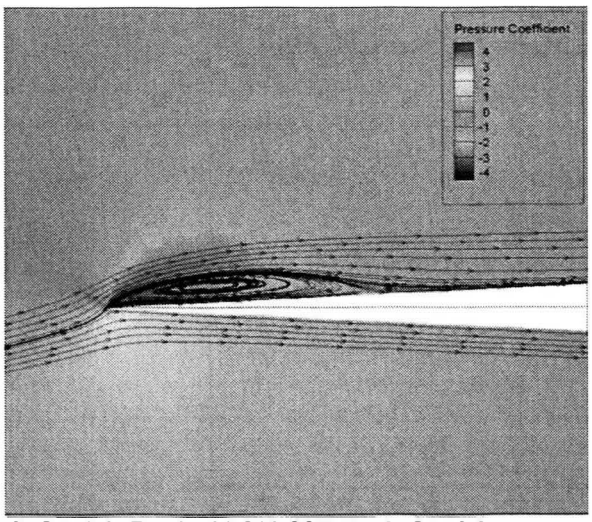


d) M=0.3, Re=2,130,803 SST Turb. Model

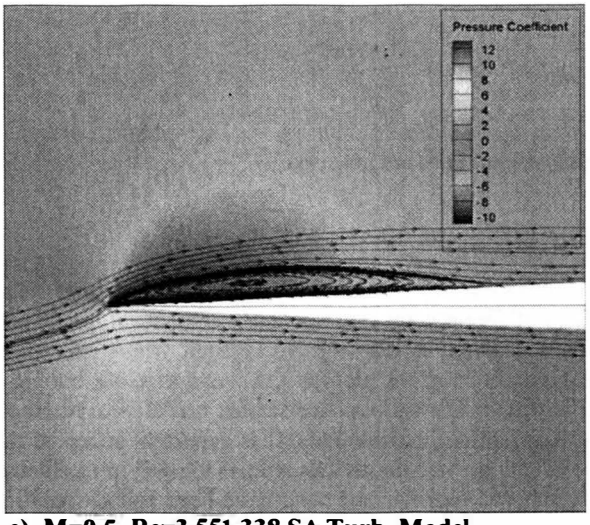


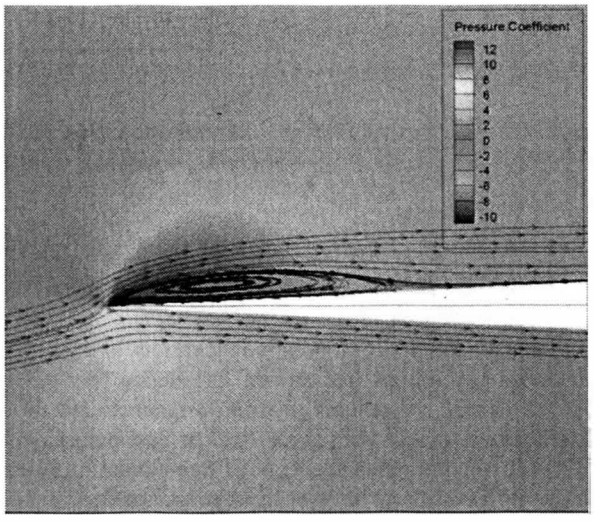


e) M=0.5, Re=3,551,338 SA Turb. Model

**Figure 4. Pressure Coefficient Contour Plots and Streamlines.**

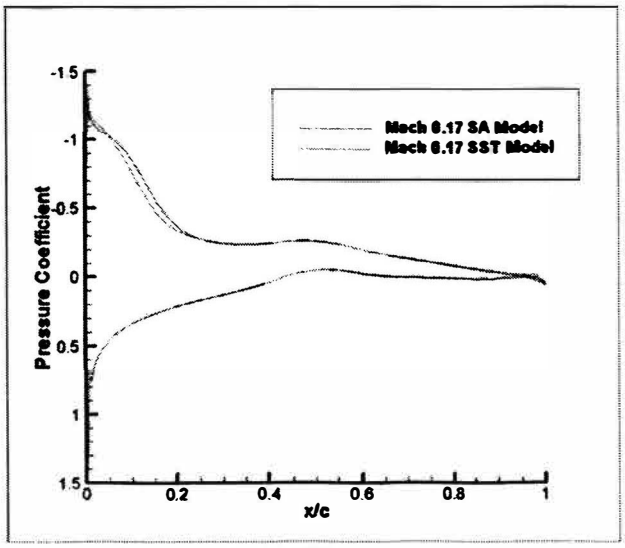


a) Mach=0.17, Re=1,207,455

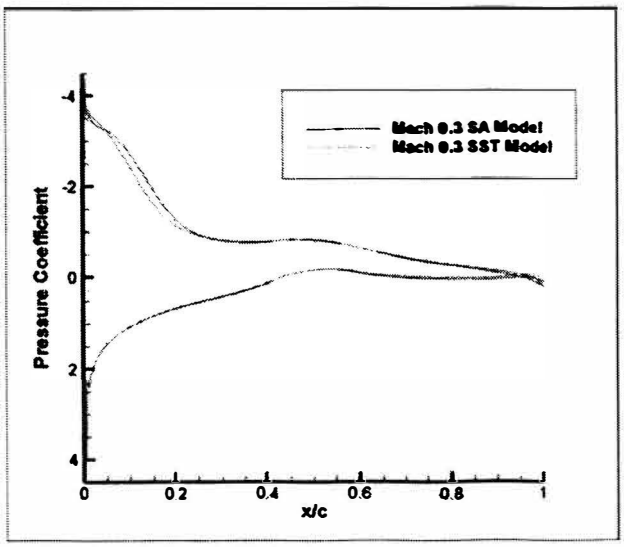


b) Mach=0.3, Re=2,130,803

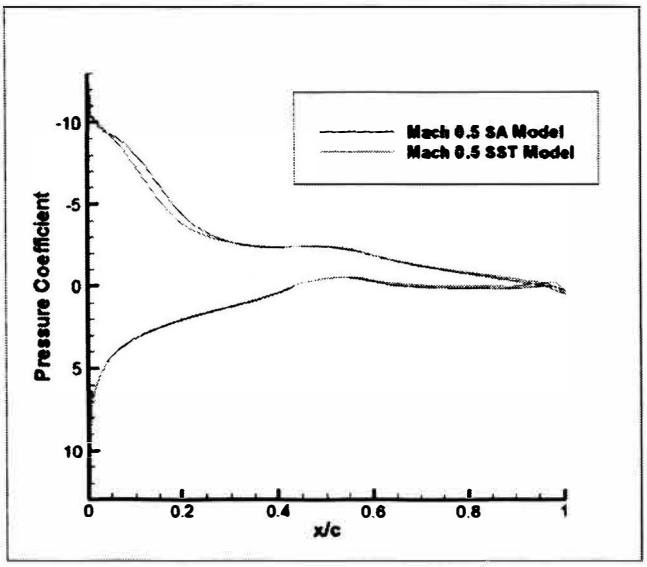


c) M=0.5, Re=3,551,338

**Figure 5. Pressure Coefficient Plots (surface pressure).**

### B. Free-stream Turbulence Effects

The second goal of the project was to evaluate the effect of free-stream turbulence on LSB development. Both $C_P$ plots contained in Fig. 6 include a variety of data sets, as is apparent by the included legends, where each data set represents a different free-stream turbulence level. Also apparent in these plots is the trend that the bubble and associated surface pressure profile do not respond to variations in the various free-stream turbulence parameters. This does not match with theoretical or past experimental (qualitative) expectations. It is generally accepted that a LSB will respond when the level of free-stream turbulence is changed.[2] All previous studies located in the literature survey of this project have been in reference to standard cambered airfoils, and none have been found specifically pertaining to supersonic airfoils. Despite this fact it is assumed that similar trends should be observed with respect to free-stream turbulence. Assuming this fact, it appears that the method used to model free-stream turbulence is in error. Significant research has been performed to identity these issues and the results follow.

The Spalart-Allmaras turbulence model uses the turbulent viscosity ratio to modify the level of free-stream turbulence present in the flow. It was initially desired to relate this ratio to turbulence intensity (I), however, several instances were found where this parameter seemed to operate completely independent of turbulence intensity (I).[8]

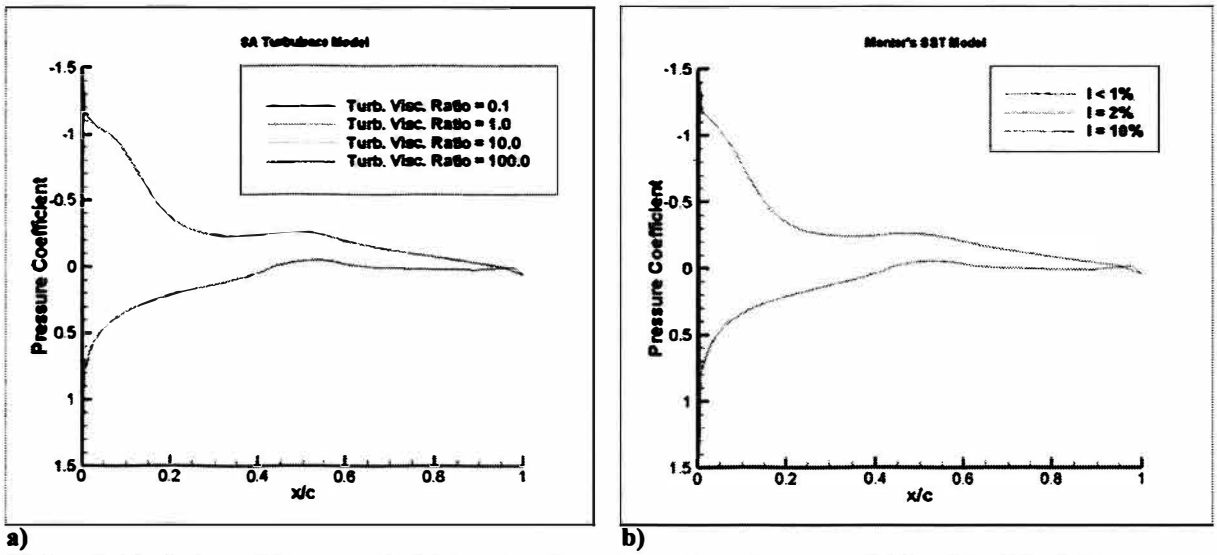


a) b)

**Figure 6. Variation of Pressure Coefficient (surface pressure) vs. Normalized Chord for M = 0.17.**
*a) SA Turbulence Model b) Menter's SST Model*

In Ref. 8 it is shown that for a certain value of I, several values of the turbulent viscosity ratio are possible. This being the case, it was difficult to get a feel for how the ratio would affect the turbulence in the flow although a reasonable range of values was known as stated in an earlier section. No documentation or past studies were located that utilized this parameter to modify the free-stream turbulence levels in a flow. It is believed that this ambiguity in the turbulent viscosity ratio may have lead to the inability of the SA model to appropriately model the free-stream turbulence, and further investigation needs to be performed.

The Menter's SST model, as shown in a previous section, has direct relations between the utilized turbulent kinetic energy and turbulence intensity. This relation between parameters allowed for the inputs to be determined more accurately than with the SA model. Figure 7a (next page) shows the turbulent kinetic energy (k) present in the flow, and Fig. 7b shows the turbulent kinetic energy dissipation parameter. The run illustrated in Fig. 7 was performed with a free-stream, non-dimensionalized k of 0.0006 (I=2%), and it can be seen that the value of k in the free-stream is closer to 0.0002 (non-dimensional k as described earlier). The higher values of k (>0.001) indicated in the legend exist in and around the LSB region on the airfoil. From these figures it appears that all of the kinetic energy being deposited in the free-stream inflow boundary of the computational domain is being dissipated. There should exist a region of higher kinetic energy (k) around the outer boundary of Fig. 7a, and the whole computational domain should have significantly higher values as well. By the time the flow reaches the airfoil the turbulence levels are very low, as if no free-stream turbulence was present. The dissipation explanation is consistent with the results gained, and is believed to be a plausible explanation. Further research needs to be conducted to verify this explanation and to find a solution. Note: The upper, rear region of the computational domain in the epsilon plot contains does not show any significant turbulence dissipation. This is due to the fact that the airfoil (and accordingly the grid) were run at $\alpha = 4°$. As such, the free-stream flow does not enter in this region of the outer boundary and correspondingly no turbulent kinetic energy is deposited here.

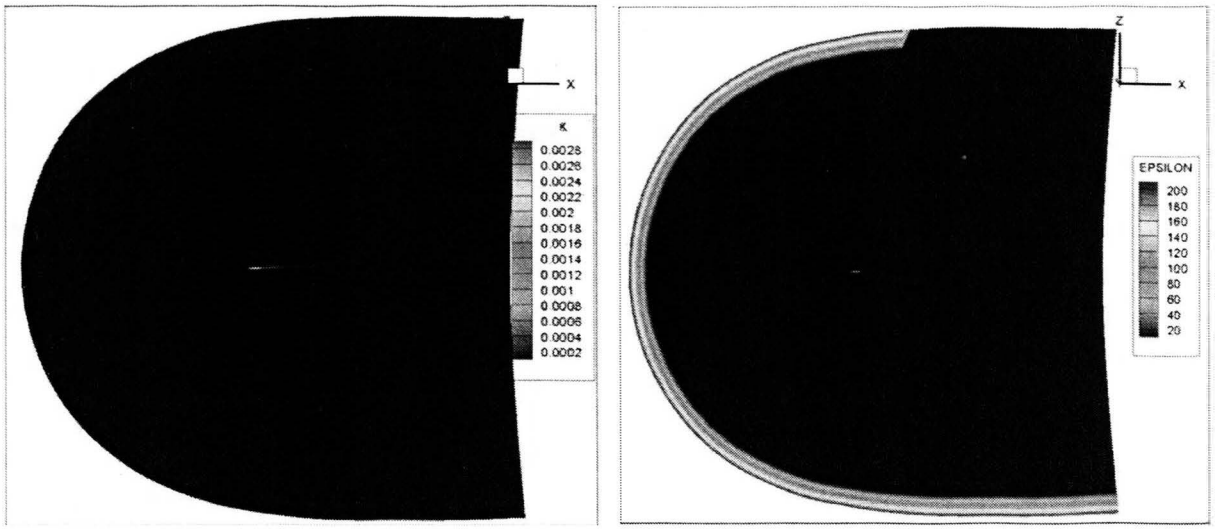


**a)** **b)**

**Figure 7. Dissipation Issue with Menter's SST ($k_\infty$=0.0006).** *a)Turbulent Kinetic Energy (k) b)Dissipation (epsilon) of Turbulent Kinetic Energy*

## VI. Conclusions

This project has shown that a significant dependence on the turbulence model chosen in a CFD analysis exists. The two turbulence models utilized in this project were successfully compared in their ability to model LSBs, but agreement between the turbulence models regarding the dimensions of the LSB modeled was not observed. The question of which turbulence model to believe is one that faces all CFD analysis projects. Validation of the conclusions obtained in this analysis will only come by comparison to a reliable and expansive experimental database. While a quantitative analysis is not yet possible, qualitative trends can be observed. In both models the LSB responded to changes in Mach and Reynolds number. As the Mach and Reynolds number were increased the length of the bubble was increased. The amount of this increase is where the discrepancies between turbulence models begin. The methods utilized in this study can not be employed to model free-stream turbulence in a desirable way. Effects such as kinetic energy dissipation are too great with the current analysis setup. The turbulence models utilized need to be changed or the way in which they are employed needs to be modified. This selection and or modification will be the subject of future research.

## Nomenclature

| | | |
|---|---|---|
| $\infty$ | = | denotes a free-stream condition when used as a subscript |
| $\alpha$ | = | angle of attack (4°) |
| $\mu_t$ | = | turbulent eddy viscosity |
| $\mu$ | = | molecular dynamic viscosity (3.7373e-7 slug/ft·s) |
| $(\mu_t/\mu)$ | = | turbulent viscosity ratio |
| U | = | velocity (composed of u, v, and w components) |
| $\rho_\infty$ | = | density (0.002378 slug/ft$^3$) |
| $R_e$ | = | Reynolds number |
| $T_\infty$ | = | static temperature (518.67 °R) |
| M | = | Mach number (free-stream) |
| $\gamma$ | = | ratio of specific heats (1.4) |
| R | = | specific gas constant (1716 ft·lb/slug·°R) |
| k | = | turbulent kinetic energy |
| I | = | turbulence intensity (%) |
| x | = | distance from leading edge to a point along the chord line |
| c | = | chord of the airfoil |
| $C_P$ | = | coefficient of pressure |

## Acknowledgments

I would like to thank the NASA Missouri Space Grant Consortium and the Opportunities for Undergraduate Research Experience (OURE) program for their funding and support during this project. I would also like to thank Dr. Fathi Finaish and the Aerospace Engineering Department at the University of Missouri-Rolla for the opportunity, guidance, and education they have provided me the past four years.

## References

[1]Norton, K. E., "A Computational Study of the Flow Fields around Supersonic Airfoils at Low Subsonic Speeds," Master's Thesis, Mechanical and Aerospace Engineering Department, University of Missouri-Rolla, Rolla, MO, 2006

[2]Schmidt, G.S., O'Meara, M.M., and Mueller, T.J., "An Analysis of Separation Bubble Transition Criteriaon at Low Reynolds Numbers," *Proceedings of the Conference of Low Reynolds Number Airfoil Dynamics*, Notre Dame, IN, June 16-18, 1985.

[3]Spalart, S.A., and Allmaras, S.R., "A one-equation turbulence model for Aerodynamic Flows," *30th Aerospace Sciences Meeting & Exhibit*, AIAA, Washington, DC, 1992.

[4]Menter, F.R., "Two-Equation Eddy-Viscosity Turbulence Models for Engineering Applications," *AIAA Journal*, Vol. 32, No. 8, 1994, pp. 1598, 1605.

[5]AGPS, Aero Grid and Paneling System, Software Package, Ver. 22.00, Calmar Research Corporation, Syracuse, NY, 2006.

[6]Chan, W.M., Chin, I.T., and Buning, P.G., "User's manual for the HYPGEN Hyperbolic Grid Generator and the HGUI Graphical User Interface," NASA TM 108791, October, 1993.

[7]Buning, P.G., Jespersen, D.C., Pulliam, T.H., Klopfer, G.H., Chan, W.M., Slotnick, J.P., Krist, S.E., and Renze, K.J., "OVERFLOW User's Manual: Version 1.8aa," NASA, April, 2003.

[8]Langtry, R.B., and Menter, F.R., "Transition Modeling for General CFD Applications in Aeronautics," AIAA 2005-522, 2005.

[9]Fluent Incorporated, "Fluent 5.5 User's Guide", Section 6.2.2, Fluent Incorporated, April 1999.